Reflection-time-of-flight spectrometer for two-electron $(e,2e)$ coincidence spectroscopy on surfaces

J. Kirschner, G. Kerhervé, and C. Winkler[a)]
Max-Planck-Institut für Mikrostrukturphysik, Weinberg 2, D-06120 Halle (Saale), Germany

(Received 29 August 2007; accepted 2 June 2008; published online 1 July 2008)

In this article, a novel time-of-flight spectrometer for two-electron-emission $(e,2e/\gamma,2e)$ correlation spectroscopy from surfaces at low electron energies is presented. The spectrometer consists of electron optics that collect emitted electrons over a solid angle of approximately 1 sr and focus them onto a multichannel plate using a reflection technique. The flight time of an electron with kinetic energy of $E_{\mathrm{kin}} \simeq 25$ eV is around 100 ns. The corresponding time- and energy resolution are typically ≈ 1 ns and ≈ 0.65 eV, respectively. The first $(e,2e)$ data obtained with the present setup from a LiF film are presented. © *2008 American Institute of Physics.* [DOI: 10.1063/1.2949869]

I. INTRODUCTION

Over the past 30 years, electron spectroscopy has become a powerful tool for the study of the electronic structure of atoms, molecules, and solids.[1–3] In addition to electron, energy loss, and photoelectron spectroscopy experiments, electron coincidence spectroscopy was established in order to study correlation effects in many-electron systems in detail.[4] Correlation effects determine many chemical and physical properties of free atoms or molecules such as acidity and reactivity.[5] In solids, these effects are manifest in the magnetic susceptibilities of metals and in superconductivity.

In electron coincidence spectroscopy two (correlated) electrons that leave the target after single photon $(\gamma,2e)$ or electron impact $(e,2e)$ are analyzed with respect to their energy and, preferentially, also their momentum.[6] Pioneering work was done by Camillioni *et al.*[7] and Weigold *et al.*[8] on a thin self-supporting carbon film and on free argon atoms, respectively. Both experiments were carried out in transmission at rather high incident energies (9 and 0.4 keV). The first successful electron coincidence experiment on a surface in a back-reflection geometry was reported by Kirschner *et al.*[9] These authors investigated the valence band structure of W(001) with low energy electrons ($E_{\mathrm{kin}} < 50$ eV) using a time-of-flight (TOF) technique. A TOF analyzer measures the time it takes a particle to travel between two particular points. The kinetic energy is calculated from the measured flight time and the particle mass. Usually, a pulsed electron or photon source is used to generate the time marker from which TOF is measured. In order to take full advantage of the TOF technique, high repetition rates and small pulse widths (typically ≈ 1 MHz and $\leqslant 1$ ns) are required. In contrast to energy analyzers, TOF analyzers permit measurement of the entire energy spectrum within a given time window. Furthermore, background is significantly reduced since it is random and therefore spread over the full TOF spectrum, and finally, data analysis is straightforward for most setups. The TOF technique is an efficient and powerful tool for determining the distribution of the kinetic energies of electrons scattered from surfaces.

In the present paper a novel TOF spectrometer is presented. The spectrometer is designed for two-electron-emission $(e,2e/\gamma,2e)$ correlation spectroscopy from surfaces at incident energies in the range of $\leqslant 50$ eV. The performance of the spectrometer was experimentally tested and coincidence measurements on a LiF film on W(001) in a back-reflection geometry were carried out.

II. APPARATUS

A. Design considerations

The central problem in electron coincidence spectroscopy is nonvalid events ("accidental coincidences") that are superimposed on the valid signal. Accidental coincidences result from the detection of two noncorrelated electrons that originate mainly from the pulsed electron source. The probability of detecting a pair of noncoincident electrons is proportional to the square of the initial electron flux while the detection probability of a coincident pair is simply proportional to the flux. For this reason it is important to have a well designed instrument that adequately suppresses uncorrelated electrons. To avoid detecting significant numbers of accidental coincidences, the incident particle rate should typically be much less than one electron per pulse on average.[10] This operation mode requires long acquisition times to obtain a TOF spectrum with acceptable statistics. Besides the incident particle rate, the solid angle of acceptance Ω of the detector also affects the count rate, particularly if the spatial distribution is isotropic. In the specific case of electron coincidence spectroscopy the coincidence rate scales on Ω^n, where $n=2$ for electron pair detection. The spectrometer design requires a careful consideration of the solid angle in this case.

The solid angle Ω that is covered by a detector (diameter $\oslash = 2a$) which is placed at a distance s away from the sample is given by $\Omega \approx \pi(a/s)^2$. In the case of a TOF experiment, on the other hand, the distance s is constrained by the minimum

[a)]Electronic mail: cwinkler@mpi-halle.mpg.de.

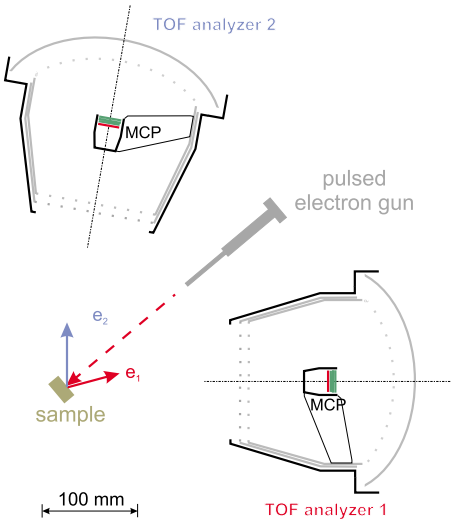

FIG. 1. (Color online) Scale drawing of the experimental setup.

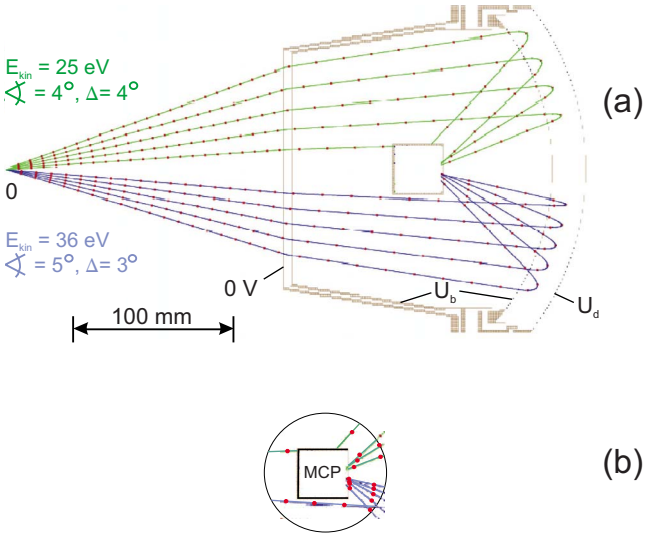

FIG. 2. (Color online) (a): SIMION simulation of electron trajectories in the spectrometer for U_b=100 V and U_d=−60 V. (b) Temporal dispersion in time at the arrival of the electrons at the MCP. The red points on the trajectories mark time differences of 3.5 ns.

value necessary for the required time- and associated energy resolution. For example, s=290 mm is required to detect a difference in energy of ΔE=0.5 eV at $E_{\mathrm{kin}} \approx 25$ eV and a TOF resolution of $\delta(\mathrm{TOF})=1$ ns. The minimum active area of the detector to cover $\Omega \approx 1$ sr at this energy resolution is $\pi 160^2$ mm^2.

This area could be accommodated with multichannel plates (MCPs), it is, however, limited by the available MCP size (maximum ≈100 mm in diameter). In the case of a large MCP, the length of the flight path from the starting point to the MCP varies significantly with the initial angle. Position sensitive MCP electronics are therefore required to determine the length of the flight path and to obtain sufficient energy resolution. For an electron coincidence experiment this solution would require two stacks of MCPs and associated electronics, which is a rather expensive solution. As an alternative to the above approach, we followed the idea to separate the collection and detection of the particles in order to have an efficient and economical setup. The design resulted in the present reflection-TOF spectrometer, where the solid angle is limited by the spectrometer entrance. The key element of the spectrometer is an electrostatic reflector which directs the collected electrons onto a small MCP and which also provides time focussing. The design is based on simulations with the software package SIMION 3D V7.0 (Scientific Instrument Services, Inc.)[11] which allows modeling of charged particle optics.

B. Detector geometry

A sketch of the present experimental setup is shown in Fig. 1. The incoming pulsed electron beam was aligned parallel to the sample normal, and two TOF-spectrometer detectors were set at angles of ±40° with respect to the primary electron beam direction. The distances between the sample and the detectors are 170 mm, and each detector accepts a solid angle of $\Omega \approx 1$ sr. The flight path from the detector entrance plane to the MCP is approximately 170 mm. The whole setup was placed in a μ-metal chamber with a base pressure of $p \leqslant 10^{-10}$ mbar. The Earth's magnetic field was compensated to a local field of <25 mG by the use of Helmholtz coils.

A more detailed drawing of the actual TOF-spectrometer detector is given in Fig. 2. Electrons (kinetic energies E_{kin1} and E_{kin2}) released from the surface due to impact of an incident electron (with the kinetic energy E_p) travel to the entrance of the spectrometer. At the spectrometer entrance the electrons pass through a grid (grid 1) which is earthed in order to maintain a field-free drift region between the sample and the spectrometer. After this grid, a second grid (grid 2) is biased at voltage $+U_b$ to accelerate the electrons to a spherical mirror which consists of a grid at potential $+U_b$ and an additional electrode at voltage $-U_d$. The electrons are reflected and focused onto a central MCP. The second grid, a conical electrode, and the spherical grid of the reflection unit are biased to the voltage $+U_b$ and form a second drift region. The transparency of each grid is ≈90%. The diameter of the MCP is 20 mm.

The spatial and temporal imaging properties of the current electrostatic lens system depend strongly on the settings of the voltages U_d and U_b. Scaling laws have been extracted from SIMION simulations to optimize time and energy resolution. The simulations were performed by calculating the trajectories of electrons traveling from a single starting point through the spectrometer to the MCP. The electrons had a fixed initial kinetic energy, but different initial angles. The voltages U_d and U_b were varied until the differences in flight times were ⩽1 ns and the incoming trajectories at the MCP were localized to a spot of ⩽8 mm in diameter. These simulations were carried out for 10 eV⩽E_{kin}⩽750 eV and established $U_b \propto (E_{\mathrm{kin}}/e)^{0.5}$ and $U_d \propto (E_{\mathrm{kin}}/e)^{0.75}$ with elementary charge e and incoming electron kinetic energy in eV. In the range of 15 eV⩽E_{kin}⩽35 eV, which is of most interest for the further discussion, U_b and U_d can be approximated as a linear functions of the kinetic energy E_{kin}:

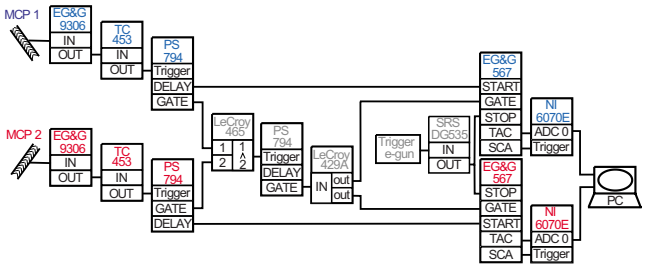

FIG. 3. (Color online) Data acquisition electronics: refer to Sec. II C for details.

$$U_b = 0.5(E_{\mathrm{kin}}/e) + 75\ \mathrm{V},$$

$$U_d = -0.6U_b.$$

These linear scalings were satisfactorily confirmed by experiment.

C. The data acquisition electronics

A sketch of the data acquisition electronics is shown in Fig. 3. Basically, the flight times of two coincident electrons are measured by a pair of time-to-amplitude converters (TACs) (EG&G/ORTEC 567). A valid event is defined by a coincidence unit (LE CROY 465). Before being fed into the coincidence unit, the incoming pulses of MCP1 and MCP2 are amplified (EG&G/ORTEC 9306) and passed through discriminators (TENNELEC TC453) which output standard Nuclear Instrumentation Module (NIM) pulses for further processing. These two NIM pulses each trigger a pair of delay generators (PS 794) which replicate the incoming pulses to (i) generate start pulses for the TACs (delay outputs of PS 794) and (ii) to define a time window according to the possible flight times of the electrons (gate outputs PS 794). The delay time and the pulse width of the gate output is typically ≈400 ns for the current setup, i.e., the current flight path length. The two gate outputs are fed into the coincidence unit, which defines a valid event for the case of an overlap between the two pulses and releases the gates of the two TACs. The output of the coincidence unit is passed through another delay generator (PS 794) that sets a gate signal of ≈650 ns pulse width. This PS 794 gate output assures that the start pulses can actually trigger the TACs and it is replicated by a fanout unit (LE CROY 429A) to control the two TACs. The TACs can only be started to perform a conversion, if the gates of the TACs have been released. After being started, the TACs are finally stopped by the trigger pulse of the electron or the light source, respectively. This latter pulse is passed through a delay generator (SRS DG535) in order to synchronize the data acquisition. The delay time at this point is ≈650 ns. The single-channel-analyzer outputs of the TACs are used to trigger analog-to-digital converter (ADC) (NI PCI-6070E) readings of the TAC output data. The ADC readings are finally transferred to the computer for further analysis. The TACs were operated to cover a time window of 500 ns and the resolution of the ADC is 12 bits. The time resolution of the acquisition electronics is 0.123 ns with these settings. This value was experimentally determined from a peak shift in the measured TOF spectrum due to an external delay which was applied to the incoming data.

III. SPECTROMETER PERFORMANCE

A. TOF and energy calibration

TOF and energy calibration were done by analyzing the peak position of the elastically scattered electrons in the measured TOF spectra while varying the energy of the incoming electrons E_{kin}. Plotting the ADC reading $\mathrm{ADC}_t \propto E_{\mathrm{kin}}^{-0.5}$ reveals a linear dependence which allows one to determine ADC_0 according to

$$\mathrm{ADC}_t = \mathrm{ADC}_0 + c_0 \frac{1}{\sqrt{E_{\mathrm{kin}}}}. \tag{1}$$

In this equation ADC_0 corresponds to the limit marking zero-flight time or infinitely high kinetic energy. The ADC reading ADC_t corresponds to a flight time of $\mathrm{TOF}=0.123(\mathrm{ADC}_t - \mathrm{ADC}_0)$ ns. Finally, from this equation one derives

$$E_{\mathrm{kin}} = c_1 \frac{1}{\mathrm{TOF}^2} \Leftrightarrow \mathrm{TOF} = \sqrt{\frac{c_1}{E_{\mathrm{kin}}}}. \tag{2}$$

It should be mentioned that each setting of U_b, U_d, or a major change in the sample position requires a recalibration. The SIMION simulation shows that maximum resolution can only be achieved for one combination of E_{kin}, U_b, and U_d, however, the experimental data give acceptable uncertainties in time of flight $\delta(\mathrm{TOF})$ and kinetic energy $\delta(E_{\mathrm{kin}})$ over a range of several tens of eV in kinetic energy.

B. TOF and energy resolution

In order to investigate the spectrometer performance the uncertainty in the time of flight $\delta(\mathrm{TOF})$ of the electrons was studied as a function of the kinetic energy E_{kin} and the grid voltages U_b and U_d. For all measurements, a pulsed electron gun was used. A pulsed electron beam is generated by periodically deflecting a continuous electron beam away from the beam axis by means of electrostatic deflectors at a frequency of (≈1.2 MHz). The pulse width of the electron gun is denoted ΔTOF. In addition to the measurements, $\delta(\mathrm{TOF})$ was also calculated analytically and simulated with SIMION.

The analytical calculation was based on

$$\mathrm{TOF} = \sum_{i=0}^{3} s_i \sqrt{\frac{m}{2E_{\mathrm{kin}(i)}}}, \tag{3}$$

by adding up the corresponding flight times TOF_i in the different sections: s_0 denotes the length of the flight path in the field free region between the sample and grid 2 at the entrance of the spectrometer, s_1 is the path length from grid 2 to the first spherical grid, s_2 the length between the two spherical grids and s_3 is the path length from the deflection grid to the MCP. The uncertainty $\delta(\mathrm{TOF})$ was calculated by assuming $\Delta\mathrm{TOF}=1$ ns and by taking into account the different possible flight paths accordingly. In the present geometry the flight path of an electron arriving at the detector edge is about 10% longer compared to that of an electron traveling

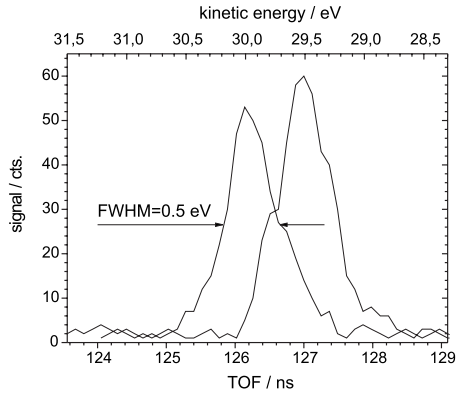

FIG. 4. Measured TOF and energy resolutions at U_b=100 V and U_d=−60 V: right curve: E_p=29.5 eV, left curve: E_p=30.0 eV. The FWHM of both distributions is comparable, 0.85 ns or 0.5 eV, respectively.

close to the centerline of the detector. Details of the SIMION simulation are shown in Fig. 2.

Figure 2(a) shows the electron trajectories within the solid angle of acceptance through the spectrometer. The electrons start at the point 0 about 170 mm away from the spectrometer entrance. They start with different angles with respect to the centerline and travel initially with kinetic energies of E_{kin}=25 eV and E_{kin}=36 eV. Starting angles are 4°–20° in increments of 4° in the case of E_{kin}=25 eV (top, green lines) and 5°–17° in increments of 3° with E_{kin} =36 eV (bottom, blue lines). The figure shows that the electrons are deflected toward the centerline after they enter the spectrometer (path s_1). This deflection is proportional to the incident angle, however, it does not depend significantly on the initial kinetic energy so long as U_b is kept higher than E_{kin}/e where e is the elementary charge. The range of angles accepted by the spectrometer is 5°–19° with respect to the centerline which corresponds to a solid angle of ≈0.5 sr. The spectrometer is blind to a solid angle of ≈0.03 sr at the centerline due to the axially mounted MCP.

While the kinetic energies of the incoming electrons do not significantly affect the path s_1 in the spectrometer, there is strong energy dependence for paths s_2 and s_3. This behavior contributes significantly to the time resolution of the spectrometer, as illustrated in more detail in Fig. 2(b) where the red dots on the trajectories are at time intervals of 3.5 ns. All intervals of the corresponding trajectory add up to the total flight time TOF from the origin 0 to the MCP, which is TOF ≈133 ns and TOF ≈119 ns for E_{kin}=25 eV and E_{kin}=36 eV, respectively. The positions of the red dots on the lower trajectories (E_{kin}=36 eV) at the MCP show that the electrons arrive at the MCP at the same time, independent of their incident angle. The position of the red dots on the upper trajectories (E_{kin}=25 eV), however, show differences in flight times depending on the incident angle; here, the flight times scale with the incident angle. The time difference between the smallest and largest accepted angle is around +1 ns. Further analysis of the time resolution of the spectrometer as a function of the parameters E_{kin}, U_b, and U_d is summarized in Figs. 4 and 5.

The experimental data in Fig. 5 (top) show a steep nonlinear decrease in δ(TOF) from ≈9 ns at E_{kin}=5 eV to

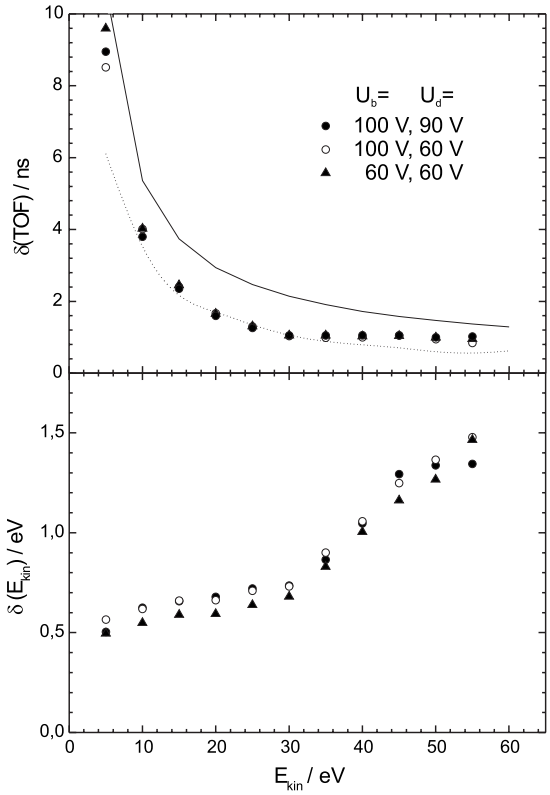

FIG. 5. Measured TOF resolution (top) and energy resolution (bottom) for different settings of U_b and U_d. In addition to the experimental data, the analytical calculation of δ(TOF) (solid line) and the SIMION data (dashed line) are shown.

≈1 ns at E_{kin}=25 eV. At higher kinetic energy the uncertainty stays constant around 1 ns, which is the pulse width ΔTOF. This observation is in good agreement with the behavior expected from Eq. (2). Applying the method of propagation of errors to Eq. (2) gives for $\delta(\mathrm{TOF}) \propto E_{\mathrm{kin}}^{-1.5}$ a nonlinear dependence which practically converges to a constant value for $E_{\mathrm{kin}} > 20$ eV. The curvatures of the data are well reproduced by the two calculated curves. While the analytical approach gives generally higher values for δ(TOF) compared to the measurements, the simulated data with SIMION fit well for $E_{\mathrm{kin}} \geqslant 10$ eV. For $E_{\mathrm{kin}} < 10$ eV the simulation fails indicating distortions in the electrical field to which slow electron are very sensitive. Figure 5 shows no significant dependence on U_b and U_d for $E_{\mathrm{kin}} > 10$ eV. For the lower kinetic energies δ(TOF) values scatter for different settings of U_b and U_d. The value of δ(TOF) is a maximum when the difference $(|U_b| - |U_d|)$ is a maximum. In this case the penetration depth of the electrons into the deflection field is rather large. The trajectories of electrons with the same kinetic energy depend strongly on penetration angle and can be very different (see Fig. 2). This also accounts for the deviation of the analytical data from the experiment. Because the deceleration in the deflection region between the two spherical grids is approximated by a mean velocity $\bar{v}_2$.

The uncertainty in kinetic energy $\delta(E_{\mathrm{kin}})$ was determined from the corresponding peak widths after converting the measured TOF spectra to energy spectra. The result is shown in Fig. 5 (bottom). Starting from low energies $\delta(E_{\mathrm{kin}})$ in-

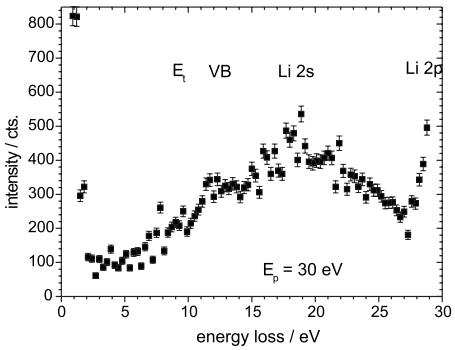

FIG. 6. Electron energy loss (EEL) spectrum of LiF/W(001).

creases slightly from 0.5 to 0.7 eV for 5 eV $\leqslant E_{\mathrm{kin}} \leqslant 30$ eV. The value of $E_{\mathrm{kin}}=0.5$ eV is quite close to the energy spread expected from the tungsten filament used in the pulsed electron gun. For $E_{\mathrm{kin}}>30$ eV the uncertainty in energy increases to $\delta(E_{\mathrm{kin}})=1.4$ eV at $E_{\mathrm{kin}}=55$ eV. The scatter of the experimental data for different settings of U_b and U_d at a given E_{kin} indicates an increasing mismatch in the combination of $(E_{\mathrm{kin}}, U_b, U_d)$ in the deflection region. If the detection of electrons with higher kinetic energy is required, it is necessary to retune the basic voltages U_b and U_d according to the scaling laws as described in Sec. II B. The experimentally achievable resolution of the spectrometer is shown in Fig. 4 which is a plot of the measured TOF (bottom scale) and the calculated energy distribution (top scale) for electron energies of $E_{\mathrm{kin}}=29.5$ eV and $E_{\mathrm{kin}}=30.0$ eV. The overall uncertainties in both cases are $\delta(\mathrm{TOF})=0.84$ ns and $\delta(E_{\mathrm{kin}})=0.5$ eV, respectively. To obtain these data the pulsing of the electron gun was set so that there was on average much less than one electron per pulse as discussed in Sec. II A. The monitored coincidence count rate in this case was $I_c \approx 1$ counts/s against a MCP count rate of $I_s \approx 1100$ counts/s.

C. Data on (*e*,2*e*) spectroscopy

The performance of the current TOF spectrometer with respect to electron spectroscopy was tested on a LiF film deposited on a W(001) single crystal. The LiF film was prepared by evaporating LiF powder from an evaporator onto the clean W single crystal. The film thickness was in the range of 7–10 ML. During the measurement the sample was held at a temperature of $T_s=120$ °C to avoid contamination and charging. The count rates I_s at the MCPs were set with respect to the coincidence count rate I_c by tuning the emission of the electron gun. By taking into account the scaling of rates of real and accidental coincidences with I_s and I_s^2, respectively, the emission was increased to the point where the ratio of real to accidental coincidences was 1:1. The resulting electron current of the pulsed electron gun is $\approx 10^{-14}$ A at a repetition rate of 1.2 MHz. Typical count rates are $I_s \approx 1500$ counts/s and $I_c \approx 3$ counts/s.

Before running a coincidence experiment, single electron energy spectroscopy was carried out on a LiF thin film. For this measurement the coincidence unit (LE CROY 465) was deactivated. Figure 6 shows an electron energy loss (EEL) spectrum taken at a primary energy of E_p =30 eV. To improve statistics, the data are summed up over 0.3 eV bins. The total number of events is ≈35 800. The EEL spectrum shows, besides the zero loss peak, two distinct peaks at ≈18 and ≈30 eV. This observation is in good agreement with data of Gołek *et al.*[12,13] for thin LiF films on W and Si substrates. The analysis of Gołek indicates that these peaks reflect the Li 2*s* state and the Li 2*p* conduction band, respectively. Another structure at ≈12 eV, much weaker compared to Li 2*s*/Li 2*p*, but also observed by Gołek *et al.*, represents the halide valence band. Due to the noise, the threshold energy E_t (or the "work function") of LiF around 10 eV is not clearly resolved against the plasmon excitations.

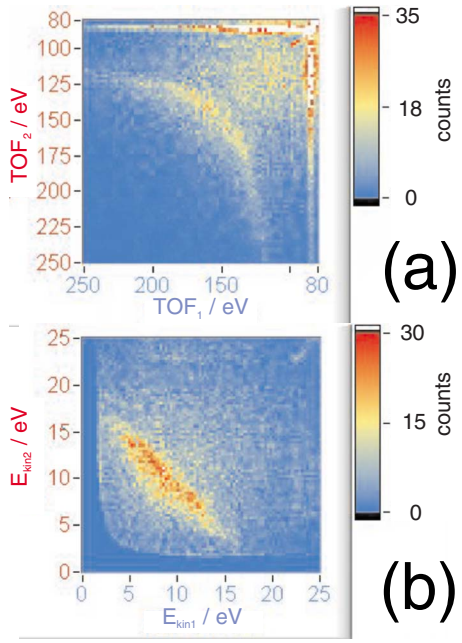

FIG. 7. (Color online) (a) 2D TOF and (b) energy spectra of LiF/W(001). The energy spectrum is plotted for $\mathrm{TOF}_{1,2}<210$ ns, which leads to the sharp cutoff at low energies.

The results of the coincidence experiment are presented in Figs. 7 and 8. Figure 7(a) shows the measured TOF distribution of the emitted electron pairs, i.e., the flight times of the two corresponding electrons are compared in a two-dimensional (2D) plot. The two straight lines of high intensity at $\mathrm{TOF}_1 \approx 80$ ns and $\mathrm{TOF}_2 \approx 80$ ns are caused by

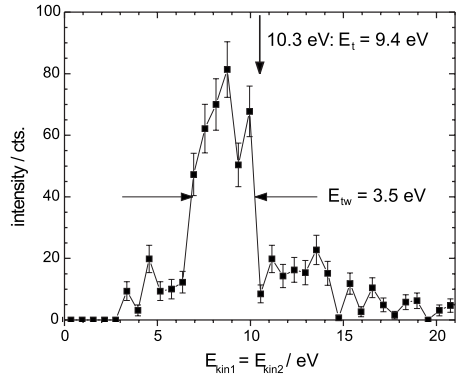

FIG. 8. Intensity distribution along the diagonal ($E_{\mathrm{kin1}}=E_{\mathrm{kin2}}$), see Fig. 7(b). The profile corresponds to the electronic structure of the LiF valence band.

accidental coincidences due to elastically scattered primary electrons. The data of Fig. 7(b) are shown on the corresponding 2D-energy distribution as calculated from Eq. (2). The complete spectra consist of about 46 500 counts in each case. To improve statistics, the TOF and energy spectra are plotted with a resolution of 2 ns and 0.3 eV, respectively. Both spectra show distinct zones of high intensity, seen as an arc and a broadened line in the TOF and energy plots. This pattern clearly indicates (i) the overall time resolution of the experiment and (ii) the signal-to-noise ratio given by the number of real compared to accidental coincidences in the energy range of interest. In more detail, this pattern can be assigned to the band structure of LiF. The minimum TOF or maximum kinetic energy is fixed by the conservation of energy according to $E_p = E_{\mathrm{kin1}} + E_{\mathrm{kin2}} + E_t$, where E_t denotes the threshold energy. The shape of the 2D-energy distribution, Fig. 7(b), is similar to the one presented by Samarin *et al.*[14] for thick LiF films. Figure 8 shows a cut along the diagonal ($E_{\mathrm{kin1}} = E_{\mathrm{kin2}}$), see Fig. 7(b), which corresponds to the electronic structure of the LiF valence (the halogen p) band. The threshold energy E_t and the full width at half maximum (FWHM) of the halide band E_{tw} agree with the UPS data reported by Poole *et al.*:[15,16] $E_t = 9.8$ eV and $E_{tw} = 3.7$ eV. The measured data indicate that a one step scattering process dominates the current coincident experiment.[17,18] Here, the incoming electron scatters inelastically with a LiF valence electron and is reflected back into vacuum from the bulk potential. The valence electron escapes from the surface, losing part of its kinetic energy to overcome the work function.

ACKNOWLEDGMENTS

We would like to thank G. van Riessen for carefully reading this manuscript.

[1] *Electron Spectroscopy: Theory, Techniques and Applications*, edited by C. R. Bundle and A. D. Baker (Academic, New York, 1977), Vol. 1.
[2] *Electron Spectroscopy for Surface Analysis*, edited by H. Ibatch (Springer, New York, 1977).
[3] G. Ertl and J. Küppers, *Low Energy Electrons and Surface Chemistry* (VHC, Weinhelm, 1985).
[4] J. Berakdar and J. Kirschner, *Many Particle Spectroscopy of Atoms, Molecule, Clusters and Surfaces* (Kluwer, Dordrecht/Plenum, New York, 2001).
[5] M. A. Coplan, J. H. Moore, and J. P. Doering, Rev. Mod. Phys. **66**, 985 (1994).
[6] I. E. McCarthy and E. Weigold, Rep. Prog. Phys. **54**, 789 (1991).
[7] R. Camillioni, A. Giardini-Guidoni, R. Tiribelli, and G. Stefani, Phys. Rev. Lett. **29**, 618 (1972).
[8] E. Weigold, S. T. Hood, and P. J. O. Teubner, Phys. Rev. Lett. **30**, 475 (1973).
[9] J. Kirschner, O. M. Artamonov, and A. N. Terekhov, Phys. Rev. Lett. **69**, 1711 (1973).
[10] O. M. Artamonov, S. N. Samarin, and J. Kirschner, Appl. Phys. A: Mater. Sci. Process. **65**, 535 (1997).
[11] For detailed information please visit the homepage of *Scientific Instrument Services, Inc.*: www.simion.com
[12] F. Gołek, Phys. Status Solidi B **177**, K5 (1993).
[13] F. Gołek and W. J. Sobolewski, Solid State Commun. **110**, 143 (1999).
[14] S. Samarin, J. Berakdar, A. Suvorova, O. M. Artamonov, D. K. Waterhouse, J. Kirschner, and J. F. Williams, Surf. Sci. **548**, 187 (2004).
[15] R. T. Poole, J. G. Jenkin, J. Liesegang, and R. C. G. Leckey, Phys. Rev. B **11**, 5179 (1975).
[16] R. T. Poole, J. G. Jenkin, J. Liesegang, and R. C. G. Leckey, Phys. Rev. B **11**, 5190 (1975).
[17] O. M. Artamonov, S. N. Samarin, and J. Kirschner, Phys. Rev. B **51**, 2491 (1995).
[18] J. Berakdar and M. P. Das, Phys. Rev. A **56**, 1403 (1997).